SANDIA REPORT

SAND2016-3819
Unlimited Release
March, 2016

Cubic Gallium Nitride on Micropatterned Si (001) for Longer Wavelength LEDs

Mark T. Durniak, Anabil Chaudhuri, Michael L. Smith, Andrew A. Allerman, S.C. Lee, S. R.J. Brueck, Christian Wetzel

Prepared by
Sandia National Laboratories
Albuquerque, New Mexico 87185 and Livermore, California 94550

Sandia National Laboratories is a multi-program laboratory managed and operated by Sandia Corporation, a wholly owned subsidiary of Lockheed Martin Corporation, for the U.S. Department of Energy's National Nuclear Security Administration under contract DE-AC04-94AL85000.

Issued by Sandia National Laboratories, operated for the United States Department of Energy by Sandia Corporation.

Available to DOE and DOE contractors from
U.S. Department of Energy
Office of Scientific and Technical Information
P.O. Box 62
Oak Ridge, TN 37831

Telephone: (865) 576-8401
Facsimile: (865) 576-5728
E-Mail: reports@osti.gov
Online ordering: http://www.osti.gov/scitech

Available to the public from
U.S. Department of Commerce
National Technical Information Service
5301 Shawnee Rd
Alexandria, VA 22312

Telephone: (800) 553-6847
Facsimile: (703) 605-6900
E-Mail: orders@ntis.gov
Online order: http://www.ntis.gov/search

SAND2016-3819
Unlimited Release
March, 2016

Cubic Gallium Nitride on Micropatterned Si (001) for Longer Wavelength LEDs

Mark T. Durniak
Department of Materials Science and Engineering
Rensselaer Polytechnic Institute
110 8th Street
Troy, New York, 12180

Andrew A. Allerman, Michael L. Smith
Advanced Materials Sciences
Semiconductor Material and Device Sciences
Sandia National Laboratories
P.O. Box 5800
Albuquerque, New Mexico 87185-MS1086

Anabil Chaudhuri, S.C. Lee, S. R.J. Brueck
Center for High Technology Materials
University of New Mexcio
1313 Goddard St SE
Albuquerque, New Mexico 87106

Christian Wetzel
Department of Physics, Applied Physics, and Astronomy, Department of Materials Science and Engineering
Rensselaer Polytechnic Institute
110 8th Stree
Troy, New York, 12180

Abstract

GaInN/GaN heterostructures of cubic phase have the potential to overcome the limitations of wurtzite structures commonly used for light emitting and laser diodes. Wurtzite GaInN (0001) suffers from large internal polarization fields, which force design compromises towards ultra-narrow quantum wells and reduce recombination volume and efficiency. Cubic GaInN microstripes grown at Rensselaer Polytechnic Institute by metal organic vapor phase epitaxy on micropatterned Si(001), with {111} v-grooves oriented along Si $\langle 01\bar{1} \rangle$, offer a system free of internal polarization fields, wider quantum wells, and smaller bandgap energy. We prepared 6 and 9 nm $Ga_xIn_{1-x}N$/GaN single quantum well structures with peak wavelength ranges from 520 to 570 nm with photons predominately polarized perpendicular to the grooves. We estimate a cubic InN composition range of $0 < x < 0.5$ and an upper limit of the internal quantum efficiency of 50%. Stripe geometry and polarization may be suitable for mode confinement and reduced threshold stimulated emission.

ACKNOWLEDGMENTS

This work was supported primarily by the Engineering Research Centers Program (ERC) of the National Science Foundation under NSF Cooperative Agreement No. **EEC-0812056, i**n part by New York State under NYSTAR contract C130145, and in part by the Sandia National Laboratories Campus Executive Fellowship for Laboratory Directed Research and Development.

CONTENTS

FIGURES

TABLES

NOMENCLATURE

LED	light emitting diode
LD	laser diode
w-GaN	wurtzite Gallium Nitride
c-GaN	cubic Gallium Nitride
QW	quantum well
GaInN	Gallium Indium Nitride
MBE	molecular beam epitaxy
MOVPE	metal organic vapor phase epitaxy
PL	photoluminescence
CL	cathodoluminescence
TE	transverse electric
XRD	x-ray diffraction
TEG	triethylgallium
TMA	trimethlyaluminum
TMI	trymethylindium
NH_3	Ammonia
SEM	scanning electron microscope
EBSD	electron back scatter diffraction
ERC	Engineering Research Center

1. INTRODUCTION

Gallium Nitride, and its alloys with Al – $Al_yGa_{1-y}N$ – and In – $Ga_xIn_{1-x}N$ – are a promising tunable bandgap material system ideally suited for high efficiency, full spectrum light emitting diodes (LEDs), laser diodes (LDs), and power transistors. GaN preferentially crystallizes in the wurtzite (w-GaN) phase on common c-plane sapphire substrates. In this orientation, however, when strained into a heterostructure with GaN, w-GaInN exhibits large piezoelectric polarization resulting in electric fields of on the order of 1-3 MV/cm.[1, 2] To achieve the emission wavelengths longer than the blue, namely green, yellow, and red, GaInN/GaN quantum wells (QWs) with InN fractions of 20-60% are needed.[3] With higher InN fractions, however, the lattice mismatch of the GaInN well to the GaN barrier increases and therefore the strain. In the consequence, the piezoelectric fields increase and reduce the wavefunction overlap of electrons and holes, thereby reducing the radiative recombination rates and leading to a lower optical output efficiency.[4] To compensate for these effects, rather narrow (~2 nm) quantum wells (QWs) are typically employed, which unfortunately also reduces the emission wavelength by means of a stronger quantum size effect. Moreover, in such thinner QWs, the volume of emitting GaInN material is reduced leading to a higher concentration of injected carrier per active volume. This in turn can activate higher order loss mechanisms by carrier-carrier interaction, such as the non-radiative Auger recombination, lowering the optical output efficiency. All these limitations should be avoided if piezoelectric polarization could be switched off in the first place. This has led to the wide exploration of epitaxial growth along various non-polar and semipolar crystallographic directions of the wurtzite crystal structure.[5–9, 10] An alternative route, growth of GaInN QWs on cubic GaN grown on micropatterned Si(001) forcing a cubic/wurtzite phase segregation, is presented here.[11,12]

Under non-equilibrium epitaxy conditions Gallium Nitride has been shown to crystallize also in the metastable cubic (c-GaN) zinc blende phase. Direct planar growth on cubic substrates has been achieved by both, molecular beam epitaxy (MBE) and metal-organic vapor phase epitaxy (MOVPE), but energetically favorable wurtzite inclusions frequently occur.[13–15] By employing micropatterned substrate on low cost Si (001) coated with SiN_x we are able to stabilize the cubic phase without wurtzite inclusions yielding cubic GaN stripes over 1 μm wide and of mm in length, on which we grew polarization-free green and yellow emitting cubic $Ga_xIn_{1-x}N$/GaN QWs.

Growth of GaN on Si could open up the market for GaN LED production. Processing time and costs would drop dramatically because the semiconductor industry already has the tools and raw materials. We have shown that GaN can be grown on the $\{111\}$ sidewalls of micropatterned Si (001), as well as that nanopatterning sapphire substrates can alleviate defect density. Combining these ideas, a nanopatterned but conventional electronic grade (001)oriented Si wafer could prove a cheap, scalable substrate for GaN growth. Our process uses standard (001)Si instead of the uncommon (111) type and a fast lithography and etching technique to form a micropatterned substrate for epitaxial growth. Initial results suggest the achievement of very low dislocation density material.

Here we present the growth and characterization of wide, 6 and 9 nm, cubic $Ga_xIn_{1-x}N$ QW samples of variable InN fraction x. From a combination of photoluminescence (PL) and cathodoluminescence (CL), we show that emission from the cubic phase GaInN dominates in the wavelength range of 520 to 570 nm without any indication of polarization electric fields within

the QW structure. We obtain a direct comparison with emission from the semipolar wurtzite $(1\bar{1}01)$ portions of the sample, over which the cubic phase exhibits at +26 nm red shift in emission for the same growth conditions. At the same time, the cubic phase emission is found to be transverse electric (TE) polarized when referenced to the long dimension of the stripe. From a detailed X-ray diffraction (XRD) analysis we attribute this to a biaxial strain condition within the wire shaped cubic stripe geometry.

2. EXPERIMETNAL PROCEDURE

Substrate preparation starts with conventional Si(001)wafers coated with a 200 nm SiN_x film. The Si {111} nucleation planes are prepared by etching v-shaped grooves (v-grooves) into the coated Si (001) wafer along the $[1\bar{1}0]$ direction by help of interference lithography and a subsequent facet-selective KOH wet etch.[16] Grooves of a 0.8 μm opening and a 4 μm pitch have been used for all of the experiments reported here. Before growth, the samples are dipped in 10% HF solution to remove the native oxide and passivate the Si (111) surface. To initiate growth on the Si {111} sidewalls of the grooves, a few nanometers of AlN is deposited by MOVPE at 1150° C to prevent a Si-Ga meltback etching of the substrate. Then, standard growth conditions for regular w-GaN are employed. Triethylgallium (TEG), trimethlyaluminum (TMA), and trimethylindium (TMI) were used as the group-III sources and Ammonia (NH_3) as the group-V source.[17]

While the exposed SiN_x on the Si (001) top surface shows some irregular deposits of polycrystalline GaN, large-area epitaxial w-GaN films form on the Si {111} sidewalls of the groove. In this mode, w-GaN grows along its positive c-direction from both opposing sides of the groove. Their common a-directions lie parallel to the stripe direction, Si $[1\bar{1}0]$. Eventually the growth fronts of two c-planes of wurtzite GaN meet within the groove and become indistinguishable from the {111} planes of the cubic phase. It is at this point where cubic growth commences along the c-GaN [001] direction, vertically up, parallel to Si [001].[11] Simultaneously, as evident from an SEM analysis of samples at various stages of the growth (not shown here) while the c-GaN is growing up vertically, the cubic crystal expands from individual nucleation sites also along the groove direction via step-flow growth of {111} planes. The cubic growth eventually fills the volume of the groove between the wurtzite layers. After sufficient time has passed to allow the groove to be completely filled, here 6000 seconds, a 6- or 9-nm wide GaInN single QW is grown at a lower temperature, 600—700° C, followed by a thin, 10 nm, GaN protection layer. All samples at a given well width share the same flow rates of the precursors. Only temperatures were varied. The final top surface of the sample consists of stripes of cubic GaN (001) flanked by wurtzite GaN $(1\bar{1}01)$ and polycrystalline GaN between these stripes. The crystallographic orientation of the c-GaN matches that of the Si substrate, allowing for easy cleaving of the Si and c-GaN both along their {110} planes, a plane perpendicular to the stripe direction. This should prove suitable for the formation of smooth mirror planes of stripe laser cavities.

Several PL spectroscopy experiments were performed to characterize the material: 1) wide area averaging PL using a 325 nm HeCd laser; 2) a wide-area UV mercury lamp excitation within a UV microscope and optional linear polarizer in front of the CCD camera; 3) polarization and temperature dependent PL using a 408 nm diode laser exciting directly in the quantum wells; and 4) CL using a Gatan system attached to a Field Emission Inc. (FEI) scanning electron microscope (SEM) at 5 keV to provide a localized (~0.1 μm) excitation. XRD was obtained using a $Cu_{k\alpha}$ source and a goniometer with a Ge 220 monochromator in triple axis configuration with a point detector (Philips).

3. RESULTS AND DISCUSSION

3.1. Long wavelength emission from 6 nm QW

To test the range of attainable emission wavelengths, a structure containing a 6 nm QW was grown along a gradient of growth temperatures covering 600—700° C. This was achieved by tilting the sample, slightly elevating its leading edge 500 μm above the susceptor by a Si wafer. Figure 1 (a) shows UV fluorescence imaging under the microscope of various portions along the tilt direction.

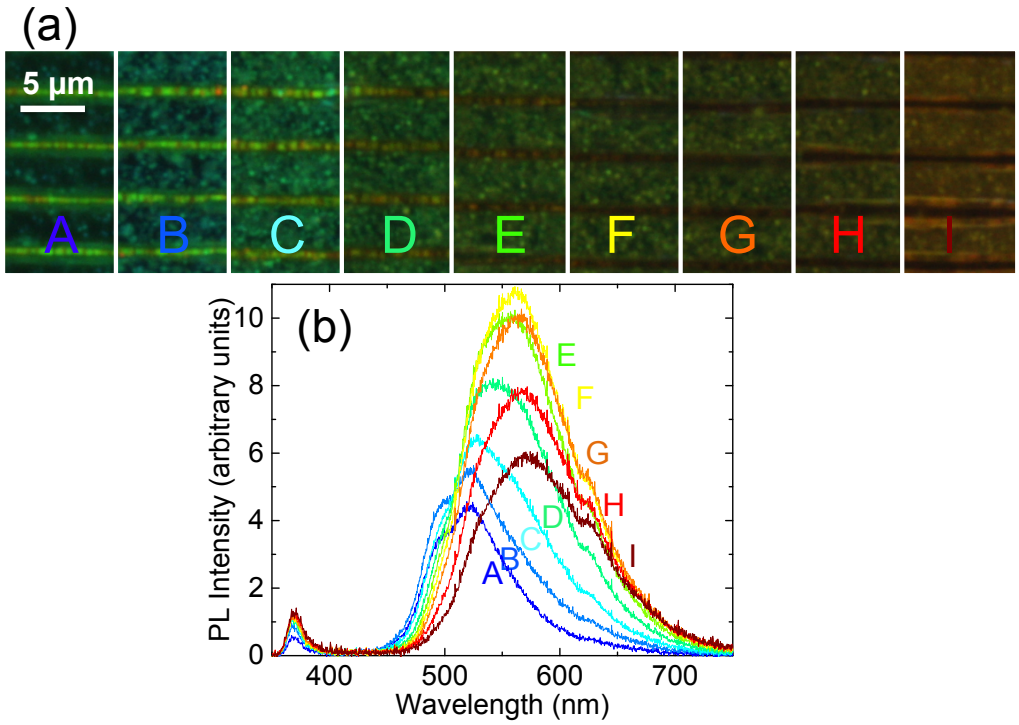

Figure 1. (a) UV microscope images of cubic GaInN samples. (b) Corresponding PL spectra.

Bright green stripes flanked by darker green on a cyan background are apparent on the hotter edge (panel A). They represent the stripes of the cubic GaInN/GaN bound by wurtzite $(1\bar{1}01)$ in the grooves and residual polycrystalline deposits between the stripes, respectively. With progression across the wafer (hot edge panel A to cold edge panel I), the stripes' emission turns from green to yellow and orange, while the background follows that color shift at some delay. In panel I, the background is orange, while the stripes appear darker. Further examination will show that they actually have a red emission. A direct reading of the actual QW growth temperature across the sample is not available, but the trailing edge of the Si substrate, which was in contact with the susceptor had a pyrometer temperature of 700° C whereas the leading edge is estimated to be about 600° C. We attribute the color grading to a higher effective InN incorporation as the growth temperature decreases from panel A to I. Figure 1 (b) shows the associated local area-averaged PL spectra (spot size ~10 μm).

A peak common to all sample locations is observed at 365 nm, which corresponds to the wurtzite bandgap. The dominating peak, however, ranges from 520 nm to 570 nm and its peak wavelength increases from panel A to I, i.e. decreasing growth temperature. We therefore collectively attribute it to the emission from the GaInN layer. The spectrum of highest intensity peaks at 555 nm, the wavelength of highest eye sensitivity. Due to the large excitation spot size, a direct spectral discrimination of the emitting crystal phases is not possible in PL. We therefore use CL with a spatial resolution of ~0.1 µm to locally excite the sample. In previous work, the locations of the cubic (001) and wurtzite $(1\bar{1}01)$ phases were identified by electron backscatter diffraction (EBSD).[18]

CL spectra of the 6 nm QW sample of region E (Figure 1 (a)) is shown in Figure 2 (a) along with an SEM image (Figure 2 (b)) indicating the respective sampling area.

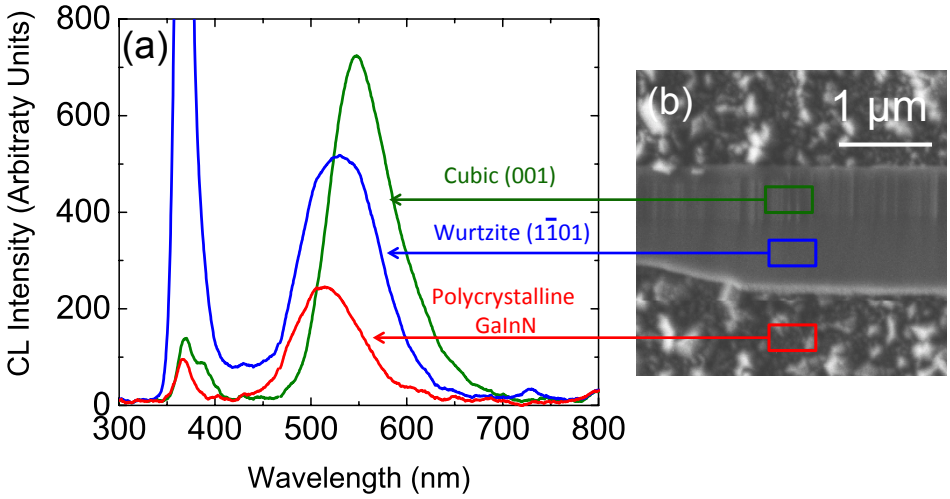

Figure 2. (a) CL spectra of the individual phases, cubic (001), wurtzite $(1\bar{1}01)$, and polycrystalline GaInN. (b) SEM image with the CL collection areas marked with boxes.

Accordingly, the cubic (001) area contributes the most intense GaInN emission at the longest wavelength of 553 nm at a width of 80 nm FWHM. This area also shows a peak at 388 nm corresponding to the cubic bandgap of 3.2 eV. The wurtzite $(1\bar{1}01)$ area shows a GaInN peak at 531 nm with a FWHM of 93 nm, somewhat larger than typical values of regular c-plane growth (~60 nm). That area also shows a strong peak at 367 nm corresponding to the wurtzite GaN bandgap. The polycrystalline GaN also shows a GaN band-edge emission at 367 nm, and a GaInN peak at 517 nm with a linewidth of 77 nm FWHM.

A correlation between local area-averaged PL peak emission wavelength and crystal phase discriminated CL peak wavelength across three locations, i.e. growth temperatures, of the wafer is provided in Figure 3.

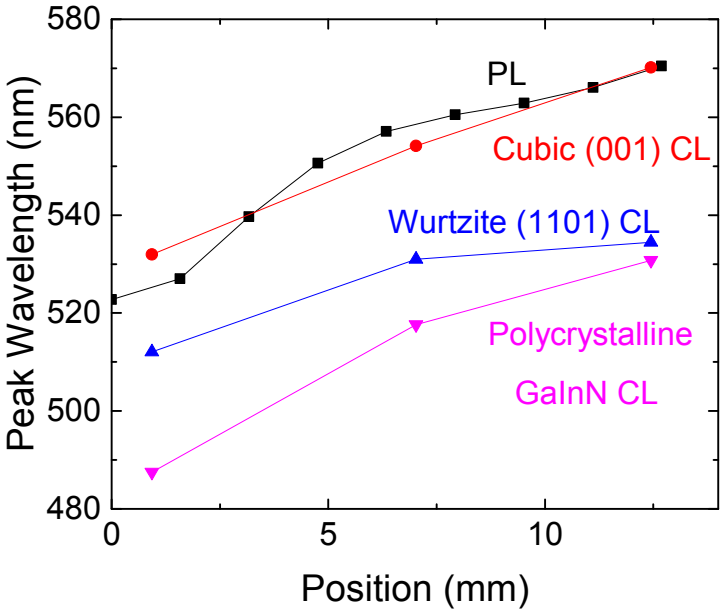

Figure 3. Peak PL wavelengths compared to the peak CL wavelengths of the different phases along the sample.

We find the PL signal to follow closely (within 4 nm) the CL signal of the cubic GaInN phase. CL of the wurtzite $(1\bar{1}01)$ follows with a blue shift of some 26 nm and the polycrystalline portions follow at a blue shift of some 40 nm. Overall, due to its higher intensity, we conclude the cubic phase GaInN emission dominates the PL emission.

In a rough approximation, the respective $Ga_xIn_{1-x}N$ alloy compositions can be estimated from the luminescence peak energies by associating them to the expected bandgap energies. Naturally, this ignores quantum size and any residual electric field effects.

For cubic $Ga_xIn_{1-x}N$ we use

$$E_{g,c-Ga_{(1-x)}In_xN} = xE_{c-InN} + (1-x)E_{c-GaN} - bx(1-x) \quad (1)$$

with E_{c-InN}= 1.8 eV, and $E_{c\text{-}GaN}$ = 3.2 eV, and b = 1.4 eV.[19]

For the wurtzite we use:

$$E_{g,w-Ga_{(1-y)}In_yN} = yE_{w-InN} + (1-y)E_{w-GaN} - by(1-y), \quad (2)$$

where E_{w-InN}= 0.77 eV, E_{w-GaN}= 3.42 eV, and b = 1.43 eV. [20] Both approximations should hold for our case of wide QWs and low, respective negligible piezoelectric fields in the cubic and $(1\bar{1}01)$ wurtzite structures. We so estimate the InN fraction in the cubic (001), wurtzite $(1\bar{1}01)$, and polycrystalline GaInN at each position CL, respectively.

In position A (hot edge) we so obtain x = 0.38, 0.27, and 0.23, respectively. In position E (middle) 0.44, 0.29, and 0.28, and 0.48, 0.30, and 0.29 in position I (cold edge). In each position, we therefore observe similar composition values for the wurtzite $(1\bar{1}01)$ and polycrystalline alloy, while the cubic phase GaInN shows substantially larger InN fractions. We

speculate that residual strain in the cubic phase could be responsible for the higher In uptake and provide a respective analysis below.

For direct correlation of the cubic GaInN wavelength with growth temperature a four-sample series of 6 nm QWs were grown at temperatures of 600, 650, 680, and 700° C (pyrometer values). UV fluorescence microscope images of these samples are presented in Figure 4 (a).

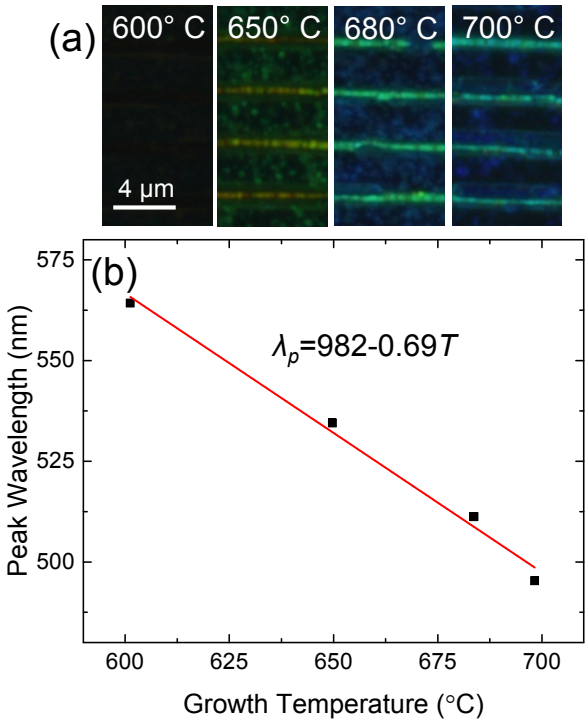

Figure 4. (a) UV microscope images of cubic 6nm GaInN QW samples grown at various well temperatures. (b) Peak PL wavelengths of 6 nm QWs compared to the quantum well growth temperature.

In each case the cubic GaInN stripe center has the brightest emission. This corroborates the findings of the tilted sample identifying the cubic (001) plane as the one dominating the structure's overall PL. The cubic stripe centers progress in color from cyan, to green and yellow as the temperature is lowered from 700 to 650° C. At the same time the polycrystalline GaN and wurtzite $(1\bar{1}01)$ change from blue to cyan to green, again exhibiting the tendency to have shorter wavelengths than the cubic (001). The sample grown at 600° C shows orange emission from the cubic stripe centers and yellow emission from the surrounding polycrystalline GaN. The PL intensity in the 600° C sample is the lowest, most likely due to decreased crystalline quality at such low growth temperatures. The samples have peak wavelengths of 564, 534, 511, and 495 nm from low to high growth temperatures and are presented in Figure 4 (b). A linear trend is observed between peak wavelength and well growth temperature with $\lambda_p = 982 - 0.69\,T$. Utilizing Equation 1, we so find the InN-fraction to vary from 0.29 in the 700° C to 0.46 in the 600° C sample in Figure 4 (a).

3.2. Polarized light emission

From a comparison of the PL intensities of the 9 nm QW sample at temperatures of 77 K and 296 K we derive an upper limit of the internal quantum efficiency in the cubic GaInN emission. We arrive at a value of about 50%, speculating that lower values are likely by comparing to PL acquired at even lower temperatures. Such a high value, together with the easily cleaving stripe geometry of the cubic GaInN/GaN structure, lends the system as a promising candidate for the development of laser diode structures. We therefore explore if a transverse electrical mode could be sustained along the cubic stripe.

To this end we analyzed the top surface emission PL using a rotating polarizer. For excitation of the GaInN layers directly, a 408 nm diode laser was used to bypass the GaN bandgap absorption. Figure 5 shows the polarization dependent, broad area PL spectra of the 9 nm QW sample, as the polarizer is rotated from 0 degrees, i.e., electric field aligned with the groove direction, to 90 degrees.

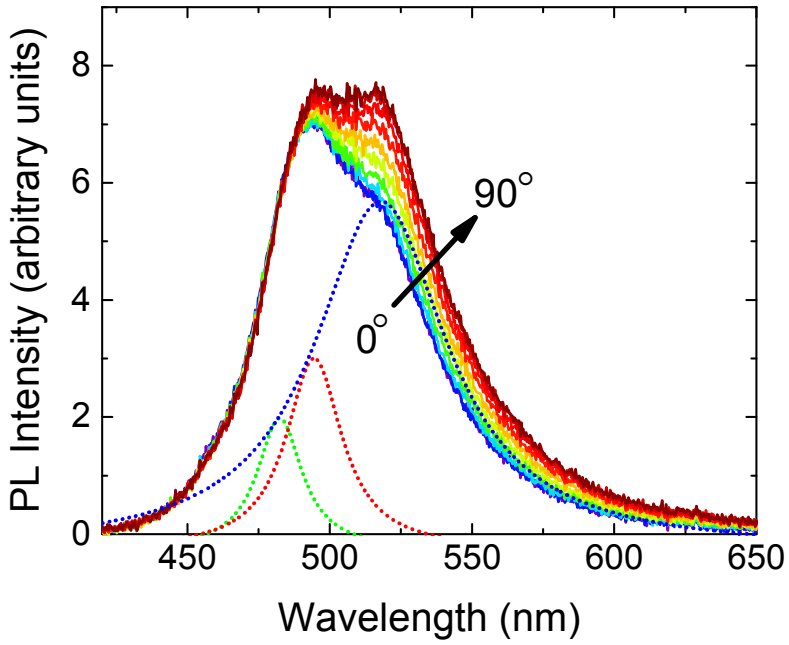

Figure 5. Polarization dependent PL from 0° to 90° (solid lines). Fitted Lorentzian curves: green, red, and blue, corresponding to the three different regions poly, wurtzite $(1\bar{1}01)$, and cubic (001) GaInN respectively (dashed lines).

The signal seems to contain multiple peaks of different behavior. We therefore performed a peak fitting with three Lorentzians, centered at the CL wavelengths of the three phases: cubic (517 nm), wurtzite $(1\bar{1}01)$ (494 nm), and polycrystalline GaInN (482 nm). One such fit is shown in dashed lines in Figure 5. In the next step we vary intensities and line widths of the wurtzite and cubic modes to fit the full rotation spectra. Since we don't expect a polarized emission from the polycrystalline material, we do not vary its contributions.

Resulting peak intensities of the cubic, wurtzite and polycrystalline GaInN are shown versus polarization angle in Figure 6.

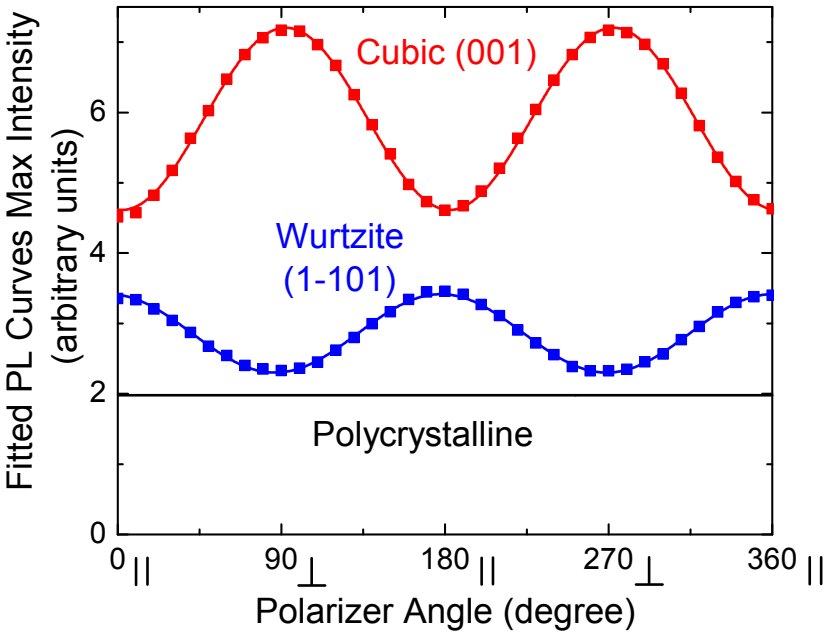

Figure 6. Maximum intensity of the fitted PL curves vs. polarizer angle; parallel and perpendicular to stripe orientation.

We find that maxima for the cubic and the wurtzite oscillate in opposite directions. The cubic has a maximum for an electric field orientation perpendicular to the stripes, while there the wurtzite has a minimum.
The oscillations can be fit by sine functions:

$$I_{(001)} = 4909 + 1294\sin\left(\frac{\pi}{90°}(\theta - 47°)\right)$$
$$I_{(1-101)} = 2895 + 557\sin\left(\frac{\pi}{91°}(\theta - 132°)\right)$$

Where θ is the angle of the polarizer with 0° referring to the electric field aligned parallel to the long stripe direction. The phase shift, φ, between the two is
$\varphi = \frac{132°\pi}{91°} - \frac{47°\pi}{90°} = 0.93\,\pi$
roughly π, or 180°, i.e. opposite phase.

The degree of polarization is represented by the polarization ratio $\rho = \frac{I_\perp - I_\parallel}{I_\perp + I_\parallel}$, where $I_{||}$ and $I_\perp$ are the intensities through a linear polarizer aligned parallel and perpendicular to the stripes, respectively. Polarization ratios of ρ = 0.23 and ρ = -0.20 are obtained for the cubic (001) and wurtzite $(1\bar{1}01)$, respectively. The negative value of the polarization ratio indicates that emission from the cubic (001) and wurtzite $(1\bar{1}01)$ are orthogonally polarized. Emission from the semipolar wurtzite $(1\bar{1}01)$ plane has been shown in literature to be polarized along the a-direction of the crystal due to a valance band splitting caused by strain.[21] This agrees with the fitted

polarization dependent PL spectra in Figure 6 and polarization dependent UV microscopy images on our samples (not shown here). Intensity of the semipolar wurtzite $(1\bar{1}01)$ has a maximum when the polarizer is oriented in the $[\bar{1}10]$direction along the stripe, parallel to the a-direction. The cubic (001) emission is slightly polarized perpendicular to the groove, obtaining maxima when the polarizer is at 90, and 270 degrees. The possibility of polarization by internal reflection from the grooved structure must be excluded since it should polarize the cubic emission parallel to the groove, opposite to the observation. This polarized emission from the cubic phase GaInN rather suggests a biaxial strain condition within the growth plane.

3.3 Stress-strain analysis by x-ray diffraction

To test for biaxial strain and assess crystal quality, we used XRD of the well aligned and oriented regrown GaInN stripes. We so resolve lattice constants along, and perpendicular to the groove. 2 θ/ω XRD patterns of the stripes are shown in Figure 7 with peak assignments in Table 1.

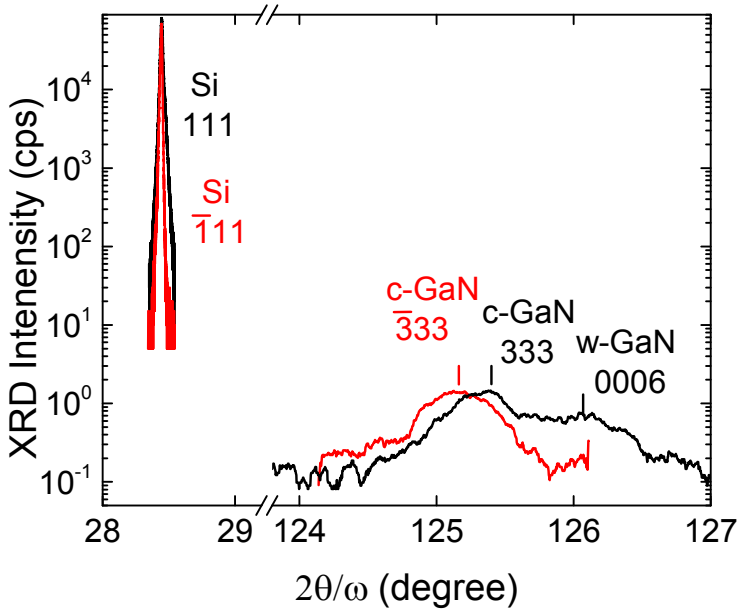

Figure 7. X-ray diffraction of the planes perpendicular and parallel to the stripe direction

Table 1. Identified planes with their XRD 2θ values and calculated d-spacings

Material – Plane *hkl*	2θ [°]	d_{khl} **[nm]**
c-GaN 002	40.048	0.2249
c-GaN 333	125.463	0.0867
c-GaN $\bar{3}33$	125.161	0.0868
Si 111	28.445	0.3135
Si $\bar{1}11$	28.442	0.3135
w-GaN 0002	34.559	0.2593
w-GaN $10\bar{2}1$	48.064	0.1891

The Si 111 diffraction angle measuring along the grooves and Si $\bar{1}11$ perpendicular to the grooves agree well with that of the unstrained bulk substrate.[22] Near 125° we find the c-GaN 333 family and w-GaN 0006 diffractions. Due to the growth geometry the w-GaN 0006 diffraction is only accessible when the beam path is parallel to the stripe direction. The similar 2θ positions of the 333 and 0006 diffractions reflect the close matching of the cubic $[111]$ direction to the wurtzite $[0001]$ direction in GaN. Fully relaxed, the 2θ positions should be equal, but a residual strain between the cladding wurtzite and the cubic core exists. The c-GaN $\{333\}$ family diffractions are further found split into a 333 along and $\bar{3}33$ perpendicular to the grooves. This lends itself to the following quantification of the strain.

From the identified XRD diffractions we can quantify residual strain within the epitaxial layers with growth direction lattice constant a_z relative to the in-plane (a_x and a_y) values. By way of Bragg's law we yield the different inter-planar spacings (d_{hkl}). From d_{333} and d_{002} we find the (001) face diagonal in the $[110]$ direction, denoted as $x_{[110]}$= 0.6371 nm, perpendicular to the grooves. From d_{333} and d_{002} we find the (001) face diagonal in the $[\bar{1}10]$ direction, $x_{[110]} =$ 0.6384 nm, parallel to the grooves, and $a_z =$ 0.4499 nm from d_{002}. Pythagorean theorem allows us to calculate the relative in-plane (a_x and a_y) values from the face diagonals. We find $a_x = a_y =$ 0.4509 nm. This shows that in-growth plane lattice constants a_x and a_y are equal and slightly larger than the out-of-plane lattice constant a_z. Furthermore, $a_z < a_0 < a_x = a_y$, where $a_0 =$ 0.4503 nm is the theoretical and reported experimental value, and $\sqrt{2}a_0 < x_{[110]} < x_{[110]}$ where $\sqrt{2}a_0$ is the relaxed face diagonal value.[23,24] This shows that the cubic GaN is under asymmetric biaxial tensile stress within the (001) plane. The cubic cell is more deformed along the groove direction than across it, specifically it is elongated more along the groove than across the groove. An anisotropic strain within the m-plane of m-plane GaN has already shown a valence level splitting leading to preferential polarization of the luminescence emission.[25] Therefore, it is most likely that the asymmetric strain here also causes a change of the valence band structure between the $[\bar{1}10]$ and $[110]$ directions. This would cause preferential recombination through the higher lying valence band resulting in polarization of the emitted light. Such a breaking of the degeneracy in the (001) plane should also reduce the relevant density of states in the valence band and therefore could result in lower inversion thresholds for the achievement of stimulated emission in a laser diode. The cubic GaN/GaInN stripes can be easily removed from their optically absorbing Si substrates and cleaved perpendicularly along the $[110]$ to form ideal laser cavities.

From the experimental values of the lattice constants a relaxed cubic lattice constant (a_0') can be extrapolated by

$$a_0^{'} = a_z\left(1 - \frac{2\nu(2a_z - a_x - a_y)}{(a_x + a_y)(1+\nu)}\right) = 0.4503\ nm,$$

where $\nu = 0.352$ is the Poisson ratio obtained in first principle theory.[26] This value for $a_0^{'}$ is in agreement with both theoretical and previously reported value from literature.[23,24] Now, with help of $a_0^{'}$, the strain in the $[\bar{1}10]$ and $[110]$ directions, along and across the groove respectively, can be determined:

$$e_{[-110]} = \frac{x_{[110]} - \sqrt{2}a_0^{'}}{\sqrt{2}a_0^{'}} = 2.99 \times 10^{-3},$$

$$e_{[110]} = \frac{x_{[110]} - \sqrt{2}a_0^{'}}{\sqrt{2}a_0^{'}} = 1.05 \times 10^{-4}.$$

The average in-plane strain can be determined:

$$e = e_x = e_y = \frac{a_x - a_0^{'}}{a_0^{'}} = \frac{a_y - a_0^{'}}{a_0^{'}} = 1.10 \times 10^{-3}$$

along with the out of plane strain:

$$e_z = \frac{a_z - a_0^{'}}{a_0^{'}} = -1.19 \times 10^{-3}.$$

This leads to the in-plane tensile stress:

$$\sigma = \frac{Ee}{(1-\nu)} = 306\ MPa,$$

where E is Young's modulus, calculated to be 181 GPa.[26]

These values have to be compared to the biaxial stress and strain in w-GaN on sapphire, where values of about -1 GPa and -2×10^{-3} (negative values indicate compressive) are commonly found, respectively.[27] In wurtzite GaN biaxial compressive strain in the growth plane is thought to lead to compositional pulling, hindering the incorporation of higher concentrations of the larger indium atoms.[28] For our cubic material here exhibiting biaxial tensile stress and strain of similar magnitude as commonly found in w-GaN but of opposite sign, the opposite may be expected; namely, a higher indium incorporation that can help relieve this compressive stress. This could explain the higher calculated InN fractions for the c-GaInN wells over that of the w-GaInN. These conditions therefore should be most favorable for the achievement of higher (20-60%) InN-fraction GaInN alloys for the goal of longer emission wavelength emitters. Despite the strain, the crystalline quality of our cubic GaN is relatively good with a linewidth of 1368 arcsec FWHM for the symmetric 002 diffraction in ω-rocking curve mode. This is an improvement over previously reported values of 1856 arcsec FWHM in a 5 μm thick MBE film.[29]

4. CONCLUSION

Cubic GaN/GaInN wide single quantum wells grown on micropatterned $Si(001)$ are able to achieve wavelengths from 520 to 570 nm with an IQE of up to 50%. LED devices constructed out of such material will not be subject to the adverse effects of built-in piezoelectric polarization fields including wavelength shift and carrier separation. These wide wells will alleviate the limitations of detrimental non-radiative Auger recombination by reducing the carrier density and likely lead to an avoidance of LED performance droop. Additionally, asymmetric biaxial tensile stress could allow for even higher InN incorporation pushing the wavelengths out further to the red and cause energy level splitting in favor for lower joint density of states in the emission channels. This splitting was found to lead to preferential recombination and partial dipole polarization in the emitted light. These results therefore provide a motivation to create laser diode structures from cubic GaN that can benefit from lower threshold densities, longer wavelengths, higher efficiencies, and easier fabrication.

5. REFERENCES

1. T. Takeuchi, C. Wetzel, S. Yamaguchi, H. Sakai, H. Amano, I. Akasaki, Y. Kaneko, S. Nakagawa, Y. Tamaoka, and N. Yamada, *Appl. Phys. Lett*. **1998**, *73*, 1691.
2. A. Hangleiter, F. Hitzel, S. Lahmann, and U. Rossow, *Jpn. J. Appl. Phys.* **1999**, *38*, 3976.
3. T. Mukai, M. Yamada, S. Nakamura,. *Appl. Phys. Lett.* **2003**, *83*, 1169.
4. C. Wetzel, S. Kamiyama, H. Amano, and I. Akasaki, *Jpn. J. Appl. Phys*. **2002**, *41***,** 11.
5. T. Detchprohm, M. Zhu, Y. Li, L. Zhao, S. You, C. Wetzel, E. A. Preble, T. Paskova, and D. Hanser, *Appl. Phys. Lett*. **2010**, *96*, 051101.
6. T. Detchprohm, M. Zhu, Y. Li, Y. Xia, C. Wetzel, E. A. Preble, L. Liu, T. Paskova, and D. Hanser, *Appl. Phys. Lett*. **2008**, *92*, 241109.
7. K-C Kim, M. C. Schmidt, H. Sato, F. Wu, N. Fellows, Z. Jia, M. Saito, S. Nakamura, S. P. DenBaars, and J. S. Speck, *Appl. Phys. Lett*. **2007**, *91*, 181120.
8. A. Chakraborty, B. A. Haskell, S. Keller, J. S. Speck, S. P. DenBaars, S. Nakamura, and U. K. Mishra, *Appl. Phys. Lett*. **2004**, *85*, 5143.
9. Y-D. Lin, A. Chakraborty, S. Brinkley, H. C. Kuo, T. Melo, K. Fujito, J. S. Speck, S. P. DenBaars, and S. Nakamura, *Appl. Phys. Lett*. **2009**, *94*, 261108.
10. H. Zhong, A. Tyagi, N. N. Fellows, F. Wu, R. B. Chung, M. Saito, K. Fujito, J. S. Speck, S. P. DenBaars, and S. Nakamura, *Appl. Phys. Lett*. **2007**, *90*, 233504.
11. S. C. Lee, X. Y. Sun, S. D. Hersee, S. R. J. Brueck, and H. Xu, *Appl. Phys. Lett*. **2004**, *84*, 2079.
12. C. Bayram, J. A. Ott, K-T. Shiu, C-W. Cheng, Y. Zhu, J. Kim, M. Razeghi, and D. K. Sadan, *Adv. Funct. Mater*. **2014**, *24*, 4492.
13. N. Zainal, S. V. Novikov, A. V. Akimov, C. R. Staddon, C. T. Foxon, and A.J. Kent, *Physica B*. **2012**, *407*, 2964.
14. H. Vilchis, V. M. Sanchez-R, and A. Escobosa, *Thin Solid Films*. **2012**, *520*, 5191.
15. S. Sanorpim, N. Discharoen, and K. Onabe, *Phys. Status Solidi C*. **2010**, *7*, 2076.
16. D. Xia, Z. Ku, S.C Lee, and S. R. J. Brueck, *Adv. Mater*. **2011**, *23*, 147.
17. T. Detchprohm, M. Yano, S. Sano, R. Nakamura, S. Mochiduki, T. Nakamura, H. Amano, and I. Akasaki, *Jpn. J. Appl. Phys*. **2001**, *40*, 16.
18. C. J. M. Stark, T. Detchprohm, S. C. Lee, Y. -B. Jiang, S. R. J. Brueck, and C. Wetzel, *App. Phys. Lett*. **2013**, *103*, 23.
19. R. Goldhahn, J. Scheiner, S. Shokhovets, T. Frey, U. Köhler, D. J. As, and K. Lischka, *Phys. Stat. Sol. (b)*. **1999**, *216*, 265.
20. J. Wu, W. Walukiewicz, K. M. Yu, J. W. Ager III, E. E. Haller, H. Lu, and W.J. Schaff, *Appl. Phys. Lett.* **2002**, *80*, 4714.
21. M. Feneberg, F. Lipski, R. Sauer, K. Thonke, P. Brückner, B. Neubert, T. Wunderer, and F. Scholz, *J. Applied Physics*. **2007**, *101*, 053530.
22. M. C. Morris, H. F. McMurdie, E. H. Evans, B. Paretzkin, H. S. Parker, N.C. Panagiotopoulos, C. R. Hubbard, in *NRS Monograph 25- Section 18 Standard X-ray Diffraction Powder Patterns*, U.S. Department of Commerce/National Bureau of Standards **1981**.
23. F. Benkabou, P. Becker, M. Certier, and H. Aourag, *Phys. Status Solidi B*. **1998**, *209*, 223.
24. S. Strite, J Ruan, Z. Li, A. Salvador, H. Chen, D. J. Smith, W. J. Choyke and H. Morkoc, *J. Vac. Sci. Technol. B*. **1991**, *9*, 1924.

25. S. You, T. Detchprohm, M. Zhu, W. Hou, E. A. Preble, D. Hanser, T. Paskova, and C. Wetzel, *Appl. Phys. Express*. **2010**, *3*, 102103.
26. A.F. Wright, *J. Appl. Phys*. **1997**, *82*, 2833.
27. S.I. Cho, K. Chang, and M.S. Kwon, *J. Mater. Sci*. **2007**, *42*, 3569.
28. Y. Kawaguchi, M. Shimizu, K. Hiramatsu, and N. Sawaki, *MRS proceedings*. **1996**, *449*, 89.
29. S. N. Waheeda, N. Zainal, Z. Hassan, S. V. Novikov, A. V. Akimov, and A. J. Kent, *Appl. Suf. Sci.* **2014**, *317*, 1010.

DISTRIBUTION

4 Lawrence Livermore National Laboratory
Attn: N. Dunipace (1)
P.O. Box 808, MS L-795
Livermore, CA 94551-0808

1	MS1086	Andrew Alleman	1126
1	MS1086	Michael Smith	1126
1	MS0899	Technical Library	9536 (electronic copy)
1	MS0359	D. Chavez, LDRD Office	1911


Sandia National Laboratories